

Disorder- and Field-Induced Antiferromagnetism in Cuprate Superconductors

Markus Schmid,^{1*} Brian M. Andersen,² Arno P. Kampf,¹ and P. J. Hirschfeld³

¹*Theoretical Physics III, Center for Electronic Correlations and Magnetism,
Institute of Physics, University of Augsburg, D-86135 Augsburg, Germany*

²*Niels Bohr Institute, University of Copenhagen,
Universitetsparken 5, DK-2100 Copenhagen, Denmark*

³*Department of Physics, University of Florida, Gainesville, FL 32611, USA*

(Dated: July 9, 2021)

Abstract

The underdoped high- T_c materials are characterized by a competition between Cooper pairing and antiferromagnetic (AF) order. Important differences between the superconducting (SC) state of these materials and conventional superconductors include the d -wave pairing symmetry and a remarkable magnetic response to nonmagnetic perturbations, whereby droplets of spin-density wave (SDW) order can form around impurities and the cores of vortices. In a simple picture, whenever SC is suppressed locally, SDW order is nucleated. Within a mean-field theory of d -wave SC in an applied magnetic field including disorder and Hubbard correlations, we show in fact that the creation of SDW order is not simply due to suppression of the SC order parameter, but rather due to a correlation-induced splitting of the electronic bound state created by the perturbation. Since the bound state exists because of the sign change of the order parameter along quasiparticle trajectories, the induced SDW order is a direct consequence of the d -wave symmetry. Furthermore the formation of anti-phase domain walls is important for obtaining the correct temperature dependence of the induced magnetism as measured by neutron diffraction.

* Corresponding author e-mail: markus.schmid@physik.uni-augsburg.de

A superconductor is characterized by a Bardeen-Cooper-Schrieffer (BCS) order parameter $\Delta_{\mathbf{k}}(\mathbf{R})$, where \mathbf{R} is the center-of-mass coordinate of a Cooper pair of electrons with momenta $(\mathbf{k}, -\mathbf{k})$. The bulk ground state of such a system is homogeneous, but a spatial perturbation which breaks pairs, e.g. a magnetic impurity, may cause the suppression of $\Delta_{\mathbf{k}}(\mathbf{R})$ locally. What is revealed when SC is suppressed is the electronic phase in the absence of $\Delta_{\mathbf{k}}$, a normal Fermi liquid. Thus the low-energy excitations near magnetic impurities and in the vortex cores of conventional SC are essentially Landau quasiparticles trapped in bound states. The underdoped cuprates have been studied intensively in recent years in part because their proximity to the Mott insulator is thought to be responsible for many unusual properties, including possibly high-temperature SC itself. These systems are quite different from conventional SC, because when the pair amplitude is suppressed locally, e.g. by a vortex, a competing ordered state¹ stabilized by the proximity to the Mott state appears to emerge instead of a normal metal. This state is characterized at low temperatures T by static local SDW order with an ordering wave vector \mathbf{Q} near (π, π) , an order which is not present in the state above T_c . This was reported first in elastic neutron scattering experiments² on $\text{La}_{2-x}\text{Sr}_x\text{CuO}_4$ (LSCO), with a correlation length of several hundred Å, but has been confirmed in other underdoped cuprate materials as well.³⁻⁶ An enhancement of incommensurate static order was observed with increasing the applied magnetic field up to 14T.² Because the signal disappeared above T_c , the magnetism was attributed to the vortices; indeed, scanning tunnelling microscopy (STM) measurements⁷ on $\text{Bi}_2\text{Sr}_2\text{CaCu}_2\text{O}_{8+\delta}$ (BSSCO) were able to directly image unusual charge order near the vortex cores which is almost certainly related to the field-induced SDW detected by neutron scattering.

Hints of magnetic ordering in the SC state had been detected earlier by μSR experiments in zero field^{8,9} as a wedge-shaped extension of the “spin glass” phase into the SC dome of the temperature vs. doping phase diagram of cuprates (see Fig. 1a). Lake *et al.*² reported that an incommensurate magnetic order similar to the field-induced state was observed in zero field, too. But although it also vanished at T_c , the ordered magnetic moment in zero field had a T dependence which was qualitatively different from the field-induced signal. The zero-field signal was attributed to disorder, but the relation between impurities and magnetic ordering remained unclear. Because strong magnetic fluctuations with similar wavevector are reported at low but nonzero energies in inelastic neutron scattering experiments on these materials, e.g. on optimally doped LSCO samples exhibiting no spin-glass phase in zero field,

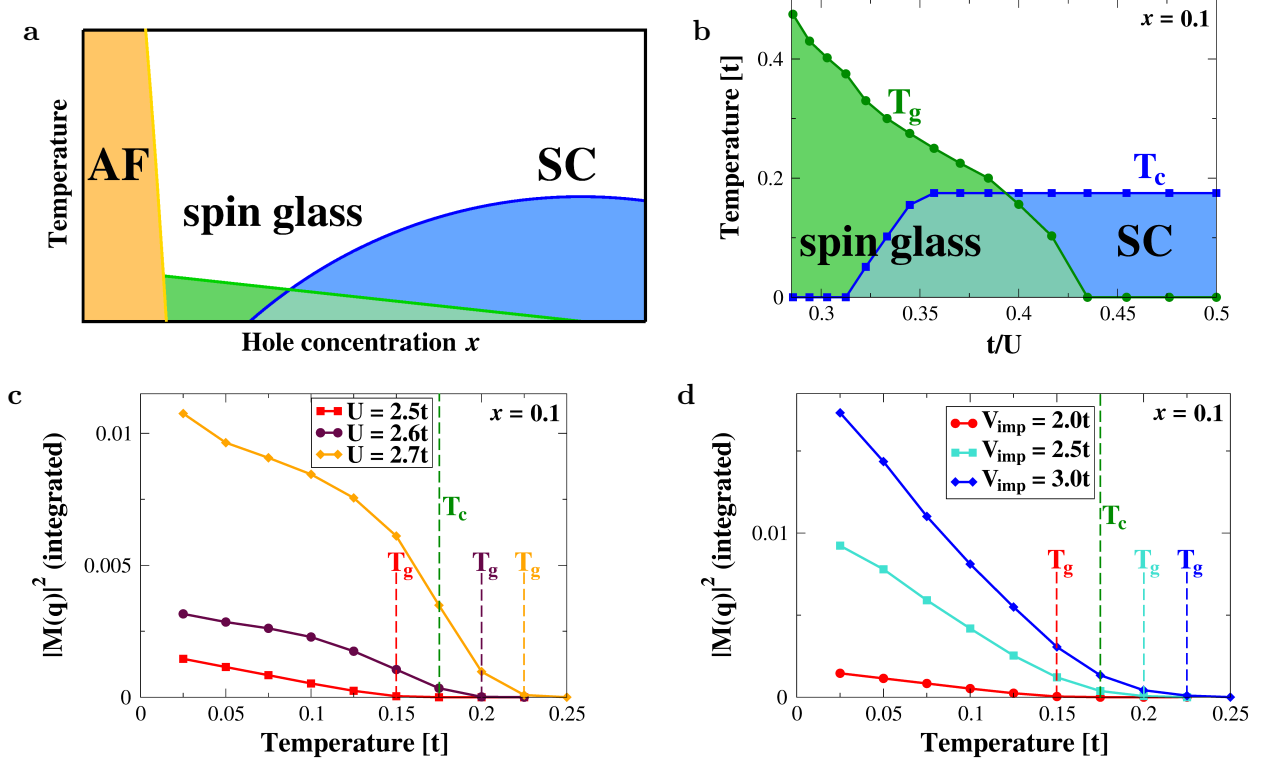


Figure 1: Phase diagrams and temperature dependence of magnetic order. **a.** Schematic temperature T vs. doping x phase diagram for cuprates. **b.** t/U dependence of the SC T_c and the disorder-induced magnetic transition temperature T_g for an impurity concentration $n_{imp} = 10\%$ with potential strength $V_{imp} = 2.0t$ and a hole concentration $x = 0.1$. t is the nearest-neighbor hopping amplitude and U denotes the Hubbard on-site repulsion. **c, d.** Magnetic Fourier component $|M(\mathbf{q})|^2$ at the ordering wavevector integrated around (π, π) vs. temperature for **(c)** different interaction strengths U (at fixed $V_{imp} = 2.0t$) and **(d)** different impurity potential strengths V_{imp} (at fixed $U = 2.5t$).

it is frequently argued that impurities or vortices simply “pin” or “freeze” this fluctuating order.¹⁰

Describing such a phenomenon theoretically at the microscopic level is difficult due to the inhomogeneity of the interacting system, but it is important if one wishes to explore situations with strong disorder, where the correlations may no longer reflect the intrinsic spin dynamics of the pure system. Such an approach was proposed by the current authors in a model calculation for an inhomogeneous d -wave SC with Hubbard-type correlations treated in mean field.¹¹ In this model a single impurity creates, at sufficiently large Hubbard interaction U and impurity potential strength V_{imp} , a droplet of staggered magnetization with a size corresponding to the AF correlation length of the hypothetical pure system.^{12–14} Such local impurity-induced magnetism has been studied extensively both theoretically and

experimentally, and was recently reviewed in Ref. 15. As was shown in Ref. 11, when these droplets come close enough to interact, there is a tendency to form incommensurate, phase-coherent Néel domains whose size is sufficient to explain the observations by Lake *et al.*² in zero field. In addition, such a model explains the empirical observations that both increasing disorder¹⁶ and underdoping⁸ enhance the SDW order.

In this paper we investigate the origin of the “order by disorder” phenomenon described in Ref. 11, as well as the T evolution of the disordered magnetic state in applied magnetic field. In the case of the field-induced SDW, an apparently very natural approach to the problem was developed by Demler *et al.*,¹⁷ who constructed a Ginzburg-Landau (GL) theory for competing SDW and SC order in a magnetic field. This order-parameter phenomenology describes correctly the reduction of condensation energy in the vortex phase of the pure SC, and leads to a phase diagram qualitatively consistent with experiments.¹ The GL approach, however, ignores the energies of the quasiparticles moving in the inhomogeneous state which also can crucially affect the competition between SDW and SC order in these materials at low T , as we show here.

In a d -wave SC without AF correlations, a bound state of an isolated vortex is found at zero energy¹⁸ due to the sign change of the order parameter on quasiparticle trajectories through the vortex core. On the other hand, solutions of the Bogoliubov-de Gennes (BdG) equations describing coexisting d -wave SC and SDW order^{19–22} show that this resonance is split by the formation of the SDW; that is, the system can lower the energy of the nearly bound quasiparticles by moving them below the Fermi energy. This finding is consistent with the STM experiments in the Abrikosov state of $\text{YBa}_2\text{Cu}_3\text{O}_{7-\delta}$ (YBCO) by Maggio-Aprile *et al.*²³ and of BSCCO by Pan *et al.*,²⁴ which observed split peaks in the vortex cores. A similar bound state is associated with non-magnetic impurities such as Zn in BSCCO and has been also imaged by STM.²⁵ It is therefore important to explore the role of quasiparticle bound states and their coupling to the SDW order to identify the origin of both types of induced local AF in the SC state. A more detailed understanding of field-induced order is also highly relevant for the interpretation of the quantum oscillations observed in recent transport experiment in high magnetic fields.^{26,27} These oscillations are possibly due to the formation of Fermi surface pockets as a consequence of SDW ordering and the concomitant reconstructed bandstructure. In addition, finding ways to understand the effects of disorder is crucial in order to reveal the intrinsic AF correlations present in the underdoped part of

the cuprate phase diagram, not least because the magnetic fluctuations at higher energies may be responsible for SC itself.

The inhomogeneous mean-field theory presented here for electrons hopping on a square lattice with a d -wave pairing potential and subject to a Hubbard on-site repulsion U , reproduces the essential aspects of the field-induced spin-glass phase shown schematically in Fig. 1a. The primary purpose of this analysis is to model the inhomogeneous SC state and does not intend to describe the Mott transition to an insulating state at half-filling; therefore the doping dependence may not be directly compared to experiment. On the other hand, if doping is assumed to be correlated with the ratio of bandwidth to local Coulomb repulsion t/U in the model, a phase diagram very much like the one found in various cuprate materials is obtained, as shown in Figs. 1b-d. We consider this a reasonable qualitative approach, since changes in the Fermi surface of these materials reported by angle resolved photoemission spectroscopy (ARPES) over the "spin glass" doping range are small,²⁸ and it is therefore plausible that the primary effect on the electronic structure is due to the correlation induced band narrowing, as discussed in Ref. 11. The phase diagram we obtain in Fig. 1b is thus comparable to the $T - x$ phase diagram shown in Fig. 1a. The magnetically ordered phase can be enhanced both by the increase of the correlation strength or stronger disorder potentials, as shown in Figs. 1c,d.

The problem studied here involves several length scales, in particular the inter-impurity separation, the inter-vortex separation, the SC coherence and the magnetic correlations lengths, which can be difficult to disentangle. We obtain results which reproduce well the qualitative aspects of the experiment by Lake *et al.*,² but show that some features depend on nonuniversal aspects of disorder, in particular the process of domain wall nucleation. While disorder- and magnetic-field induced SDW order both add to the ordered moment, the interference of disorder and magnetic-field effects is quantitatively significant. The domain wall formation proves responsible for the distinct T dependences of the field- and the disorder-induced magnetization. An intriguing aspect of the present theory is that it also includes a crossover from magnetic droplets to filamentary stripe-like structures in selected regimes of hole densities and impurity concentrations. The model therefore offers a concrete route to describe the physics of the pinning of stripe correlations in the SC state. This insight may prove relevant for many experiments in the underdoped cuprates which have been attributed to stripes.

The basis for our model analysis is the BCS pairing Hamiltonian for a d -wave SC with orbital coupling to an applied magnetic field, to which we add site-centered chemical disorder and a local Hubbard repulsion; the latter is treated in an unrestricted Hartree-Fock approximation:

$$\begin{aligned}
H = & - \sum_{ij\sigma} t_{ij} e^{i\varphi_{ij}} c_{i\sigma}^\dagger c_{j\sigma} - \mu \sum_{i\sigma} c_{i\sigma}^\dagger c_{i\sigma} + \sum_{\langle ij \rangle} \left(\Delta_{ij} c_{i\uparrow}^\dagger c_{j\downarrow}^\dagger + h.c. \right) \\
& + \frac{U}{2} \sum_i (\langle n_i \rangle n_i - \langle \sigma_i^z \rangle \sigma_i^z) + \sum_{i\sigma} V_i^{imp} c_{i\sigma}^\dagger c_{i\sigma}.
\end{aligned} \tag{1}$$

Here, $c_{i\sigma}^\dagger$ creates an electron on a square lattice site i with spin $\sigma = \uparrow, \downarrow$. The hopping matrix elements between nearest and next-nearest neighbor sites i and j are denoted by $t_{ij} = t$ and $t_{ij} = t'$, respectively. An electron moving in the magnetic field from site j to i acquires additionally the Peierls phase $\varphi_{ij} = (\pi/\Phi_0) \int_{\mathbf{r}_j}^{\mathbf{r}_i} \mathbf{A}(\mathbf{r}) \cdot d\mathbf{r}$, where $\Phi_0 = hc/(2e)$ denotes the superconducting flux quantum and $\mathbf{A}(\mathbf{r}) = B(0, x)$ is the vector potential of the magnetic field in the Landau gauge. The chemical potential μ is adjusted to fix the average charge density $n = \frac{1}{N} \sum_i \langle n_i \rangle = 1 - x$, where x is the hole concentration and N is the total number of lattice sites; in the following we will focus on $x = 0.1$. The magnitude of the d -wave pairing amplitude Δ_{ij} is determined by the strength of an attractive nearest-neighbor interaction V_d . The non-magnetic impurity potential V_i^{imp} is described by a set of pointlike scatterers at random positions, and all fields, i.e. the pairing amplitude Δ_{ij} , the local charge density $\langle n_i \rangle$, and the local magnetization $\langle \sigma_i^z \rangle$ are calculated self-consistently from the solutions of the associated BdG equations. (For further details of the numerical method we refer to the Supplementary Information.)

We start with a single non-magnetic impurity in a d -wave SC at $U = 0$. The fingerprint of the induced virtual bound state is a single near zero-energy peak in the local density of states (LDOS) (see Fig. 2a). In this situation there is no magnetization induced by the impurity. Increasing the on-site Coulomb repulsion beyond a critical value U_c , a staggered magnetization emerges in the neighborhood of the impurity (Fig. 2b). The two-sublattice nature of the magnetic pattern, in conjunction with the spatial extent of the impurity-induced resonance leads to a spin-dependent splitting of the near-zero-energy peak in the LDOS; one resonant state with a selected spin direction is thereby shifted below and the other above the Fermi energy, as is most clearly seen at the nearest-neighbor sites of the impurity where the resonant state has the largest weight (see Fig. 2a). The spin-dependent

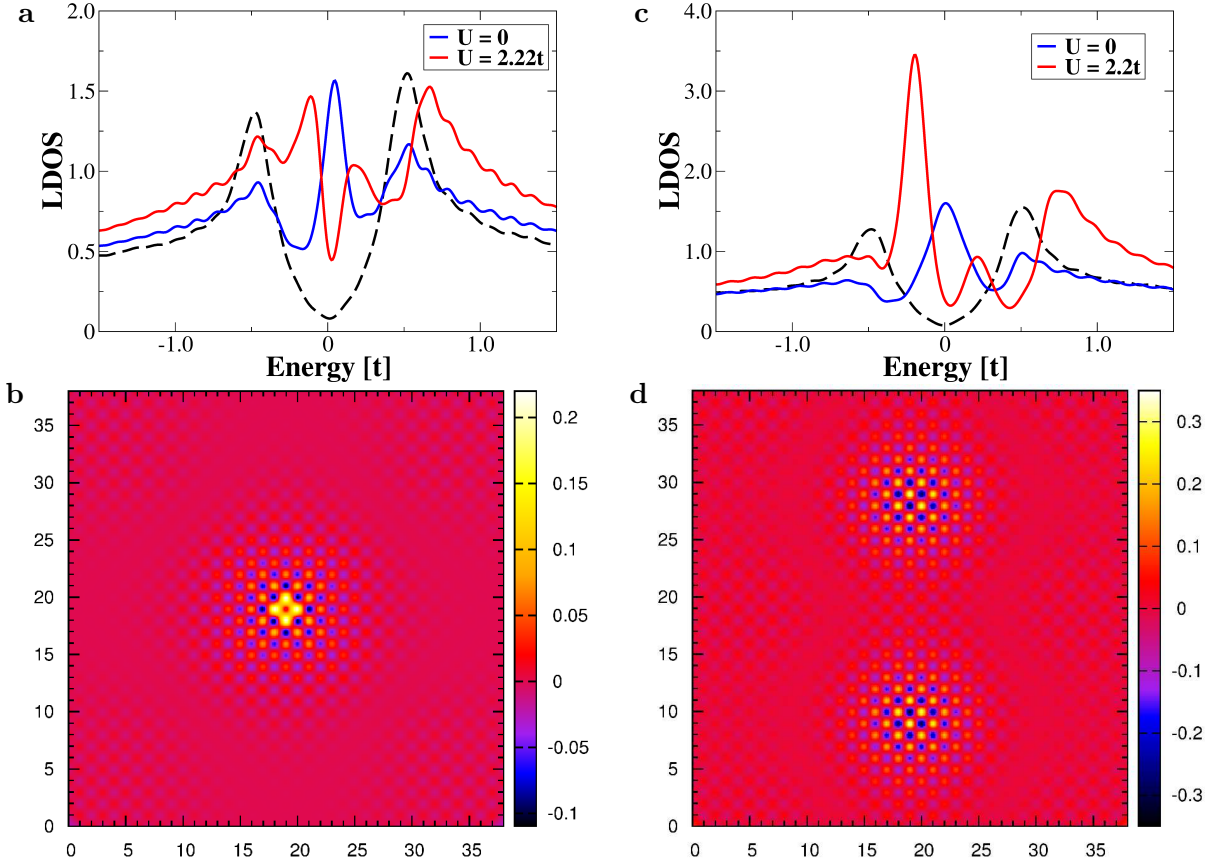


Figure 2: Impurity- and field-induced magnetization. **a, c.** Local density of states (LDOS) at a nearest-neighbor site of a single impurity (**a**) and in the center of one vortex (**c**). In both cases, above a critical U_c , local SDW order is induced, concomitantly the zero-energy peak in the absence of the Hubbard repulsion (blue curve) splits spin-dependently (red curve). The dashed curves show the clean LDOS far from the perturbation. **b, d.** Real-space patterns of the magnetization $\langle \sigma_i^z \rangle$ in units of μ_B on a 38×38 lattice for $U = 2.2t > U_c$ at low temperature $T = 0.025t$. **b** shows the magnetization nucleated by a strong impurity ($V_{imp} = 60t$) located at the center. In **d** two superconducting flux quanta $\Phi = 2\Phi_0$ thread an impurity-free d -wave SC.

splitting reduces the bound-state energy of a spin-up or -down state, and therefore stabilizes a local droplet of staggered magnetization which carries a total spin 1/2-moment surrounding the impurity. The splitting of the resonance peak can therefore be viewed as the origin of the impurity-induced magnetization. It is important to note that the splitting of the bound state is *not* due to the suppression of the d -wave order parameter near the impurity. As we have verified, the order parameter can be artificially held constant in the solution of the BdG equations, and a nearly identical result is obtained.

In the presence of a thermodynamically finite density of impurities, we recover at $T = 0$ the results of Ref. 11, i.e. the creation of a defected but magnetically ordered state

as defined by strong peaks in the Fourier transform of the local magnetization $M(\mathbf{q})$ at incommensurate wavevectors \mathbf{q} near (π, π) . The effect of temperature is now naturally included in the theory via T -dependent occupation probabilities of Bogoliubov quasiparticle states, as discussed in detail in the Supplementary material. In Fig. 1b we show the extent of the quasi-ordered phase, labelled “spin glass”, which expands as correlations increase, and disappears at a critical value of t/U which depends on the strengths of the pairing interaction and the impurity potential. The intensity of the incommensurate magnetic Bragg peaks is shown in Figs. 1c and 1d as functions of T for fixed t/U and fixed impurity potential strength, respectively. From Fig. 1c it becomes evident that the magnetic ordering, or “glass transition” temperature T_g can be smaller, equal to, or larger than T_c depending on U . In Fig. 1d we show how increasing the impurity potential V_{imp} can increase both the amplitude of the disorder-induced SDW and T_g itself. These results are consistent with the empirical observation that the size of the spin-glass phase is not universal, and in particular the critical doping beyond which magnetic order is no longer observed varies considerably between intrinsically disordered cuprates like LSCO and BSCO, and clean materials like YBCO.

The magnetization induced by an orbital magnetic field can be traced to the same microscopic origin as the impurity-induced magnetization.²⁰ Above a critical U_c a staggered spin pattern is nucleated in the vortex cores with a spatial extent reaching beyond the size of a vortex core (see Fig. 2d), as observed in experiment.² For the parameter set chosen, the core radius estimated from the area where the order parameter is suppressed is about one lattice spacing. The LDOS in the vortex center reveals that the origin of the field-induced magnetization is tied to the spin-dependent splitting of the Andreev bound state in the vortex core (Fig. 2c). The conjecture that the field-induced magnetization indeed appears simultaneously with the peak splitting in the LDOS is explicitly verified in Fig. 3. For the unmagnetized vortex at $T = 0.175t$ a single Andreev bound-state peak exists at zero energy. With decreasing T the vortices nucleate a staggered spin pattern precisely at the T where the zero-energy peak in the LDOS splits. With further cooling the peak splitting grows, more spectral weight is shifted below the Fermi energy, and the magnetization is enhanced.

The natural next step is to consider a finite density of non-magnetic impurities in the presence of an external magnetic field and to compare it to zero-field results. Specifically for the modelling of LSCO, we assume in the following that the Sr ions are the primary source

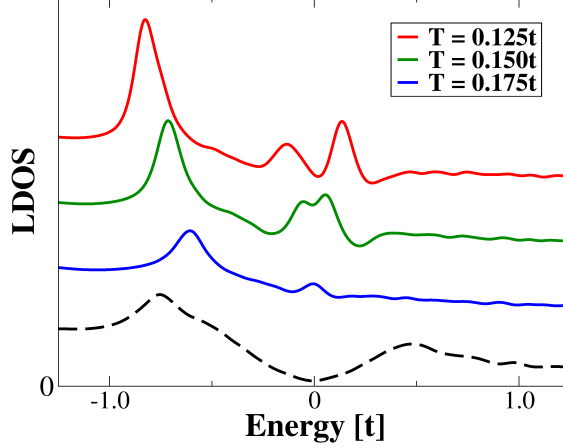


Figure 3: Temperature dependent peak splitting in a magnetic field. LDOS at the vortex center for three different temperatures below T_c in the absence of impurities. Below the critical temperature $T_g = 0.175t$, the vortices magnetize and simultaneously the Andreev bound-state peak splits. The black dashed curve shows the LDOS far away from the vortex.

of disorder, such that $n_{imp} = x$, where n_{imp} denotes the impurity concentration. These systems are in the strongly disordered regime where the AF correlation length (droplet size) is comparable to the average distance between the dopants, such that the disorder is far from the one-impurity limit. Since the Sr dopants are removed from (but close to) the CuO_2 planes, we model them as weak scatterers with $V_{imp} = 1.3t$. Figs. 4a,b show the magnetic structure factor $S(\mathbf{q})$ at a fixed temperature far below T_c in zero and finite magnetic field averaged over ten different impurity configurations. As in Figs. 1c,d, $S(\mathbf{q})$ is approximated by $|M(\mathbf{q})|^2$ with $M(\mathbf{q}) = \frac{1}{N} \sum_i e^{i\mathbf{q}\cdot\mathbf{r}} \langle \sigma_i^z \rangle$ (see the Supplementary information for details). The magnetic signal in the structure factor appears at the incommensurate wavevectors $\mathbf{q} = (\pi, \pi \pm \delta)$ and $\mathbf{q} = (\pi \pm \delta, \pi)$ (see Fig. 4a). The magnitude of the incommensurability δ however varies for distinct impurity configurations randomly selected for 22×22 lattice systems. For the weak magnetic signal in zero field the averaging over different impurity configurations is therefore imperative but computationally demanding. Applying an external magnetic field strongly enhances the magnetization and reinforces incommensurate peaks at unambiguously selected wavevectors which are robust against variations in the impurity configurations (See Fig. 4b).

Remarkably, the temperature dependence of the structure factor (see Fig. 4c) closely resembles the neutron scattering data on LSCO by Lake *et al.*² For the results shown in Fig. 4 we have chosen a parameter set where the staggered magnetization in zero field has its

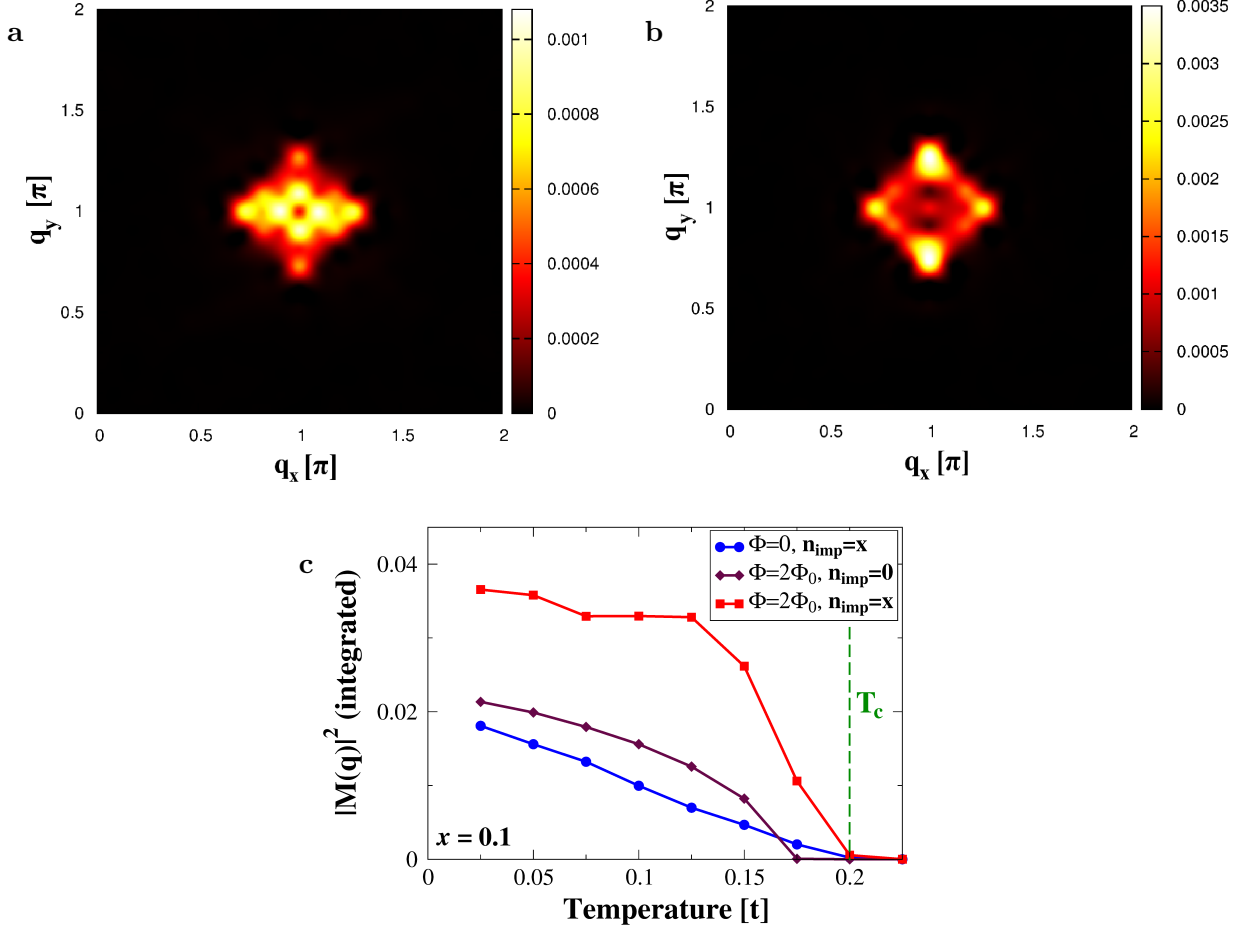


Figure 4: Averaged magnetic structure factor for a many-impurity system. **a,b.** Intensity plot of the magnetic structure factor around (π, π) at $T = 0.025t$ in zero magnetic field (**a**) and at finite field (**b**). The structure factor data were averaged over ten different impurity configurations. For the used system size of 22×22 lattice sites a magnetic flux of $2\Phi_0$ corresponds to a strong magnetic field with $H = 59T$. The impurity concentration $n_{\text{imp}} = x$ is fixed to 10% ($V_{\text{imp}} = 1.3t$) and $U = 2.9t > U_c$. **c.** T -dependence of the peak intensity integrated around (π, π) in zero-field and at finite field with the finite density of impurities $n_{\text{imp}} = x$ (blue and red curve, respectively); for the data with $\Phi = 2\Phi_0$ and $n_{\text{imp}} = x$ the zero-field data were subtracted. For comparison also the structure factor in a clean system is included for the same magnetic-field strength (purple curve). $|M(\mathbf{q})|^2$ (integrated) translates directly to the ordered spin moment squared in units of μ_B per Cu^{2+} .

onset at a temperature T_g indistinguishable from T_c . This reflects a situation where upon cooling through T_c the localized bound states inside the d -wave energy gap emerge and immediately split in the self-stabilizing staggered magnetic pattern. Towards lower T the magnetic structure factor rises in a markedly different way in zero and in finite field. While the field-induced part of the magnetic signal has a negative curvature, the zero-field magnetic structure factor increases approximately linearly upon cooling. The two mechanisms of

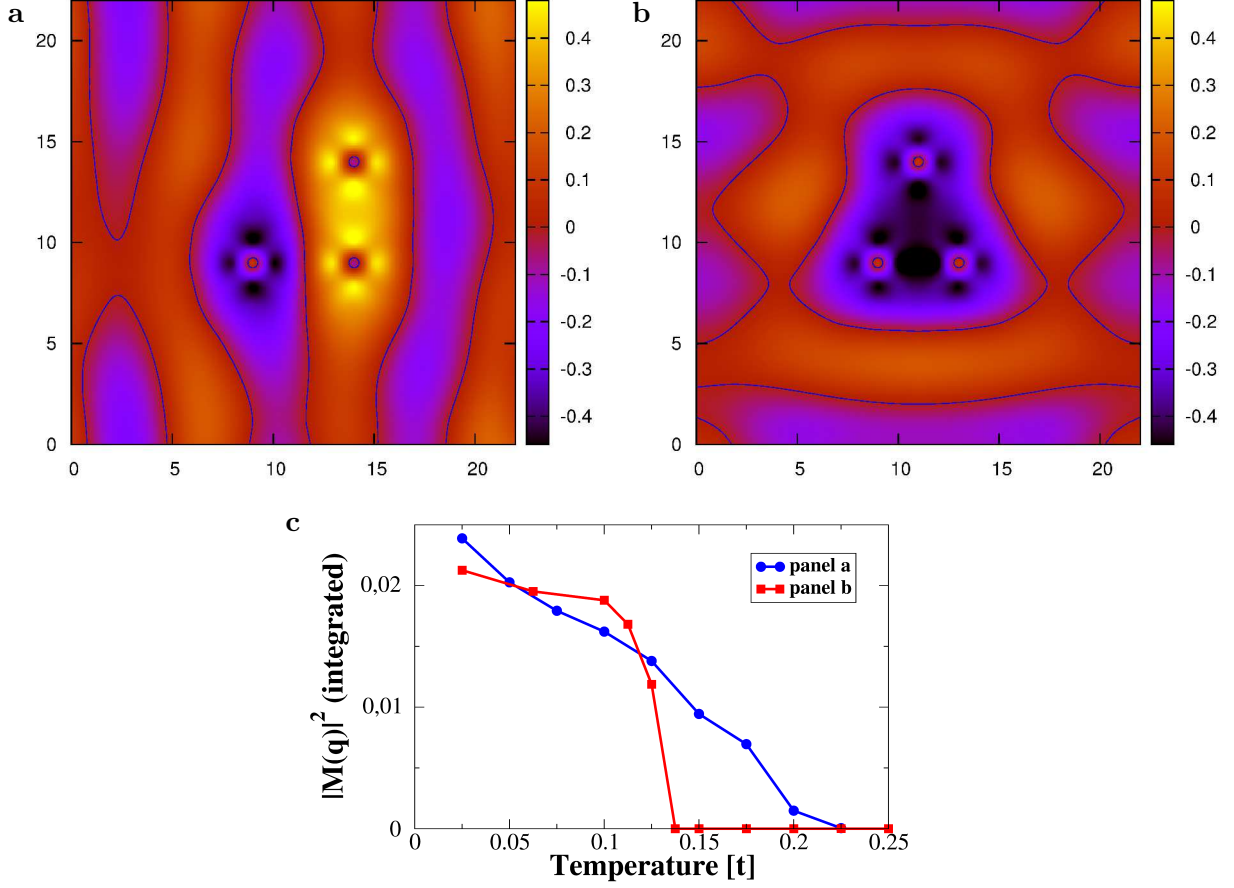


Figure 5: Anti-phase domain walls. **a, b.** Real-space image of the staggered magnetization at $T = 0.025t$ induced by three non-magnetic impurities. In impurity configuration **a** anti-phase domain walls appear vertically. In configuration **b** the staggered magnetization induced by the three impurities adjusts to a uniform AF domain around them. **c.** Temperature dependence of the integrated magnetic structure factor for the impurity configurations **a** (blue curve) and **b** (red curve), respectively.

impurity- and field-induced SDW do not simply cooperate additively; the field-induced part of the magnetization is twice as large in the presence of impurities as compared to the field-induced SDW in the clean system (see Fig. 4c). The zero-field increase of the magnetization in the inhomogeneous SC state originates from the merging of AF patches nucleated by the individual impurities. Without impurities the increasing field-induced magnetization with cooling results from the growth of the magnetized regions around the well-separated vortex cores. Thus, both our zero- and finite-field results for the finite density of non-magnetic impurities $n_{imp} = x$ closely follow form of the T dependence of the the neutron scattering data for underdoped LSCO.² Still, due to computational restrictions we are not yet able to access the low magnetic-field strengths to allow for a direct comparison with experiment.

An important remaining question is why the T dependences of the magnetization are different in zero and in finite field. A hint is provided by the observation that the T dependence of the magnetic structure factor for the impurity-free field-induced magnetization and also for just two single impurities in zero field has a negative curvature. In both cases the induced staggered magnetization patterns around each impurity or each vortex, respectively, adjust their individual two-sublattice spin structures in phase and thereby avoid any domain walls.²⁹ For three nearby impurities, however, it proves already difficult to find a specific configuration where anti-phase domain walls are absent. In Figs. 5a,b we compare the staggered magnetization of two 3-impurity configurations with distinctly different domain-wall patterns. Remarkably, placing the three impurities on the same sublattice to form a right-angled equilateral triangle as in Fig. 5a generates a sequence of vertical anti-phase domain walls. If instead the impurities are configured in an acute equilateral triangle as in Fig. 5b a simply connected AF island forms around them. As Fig. 5c shows, with decreasing T the magnetic signal evolves differently for each impurity configuration. Intriguingly, $|M(\mathbf{q})|^2$ rises almost linearly for the configuration with vertical anti-phase domain walls while it has a negative curvature for the single domain island. These examples, and others we have investigated, suggest that the linear low- T rise of the magnetic signal for a finite density of impurities in zero field originates from the anti-phase domain walls which are always present in the randomly generated impurity configurations. For the field-induced magnetization it is the larger distance between the magnetized vortices which prevents the occurrence of domain walls and therefore alters the T dependence of $|M(\mathbf{q})|^2$.

All the results presented above focused on static disorder- and field-induced SDW, but inelastic neutron scattering experiments have shown that in the SC state the spin excitations at finite energy have almost the same distribution of spectral weight in \mathbf{q} as the frozen magnetic order.³⁰ For very low doping in the normal spin glass phase above T_c , the neutron intensity pattern is rotated by 45° and the connection to the spin correlations discussed here is less obvious. In fact, the utility of our model of choice is questionable for the description of the normal state where Fermi liquid concepts may not even be applicable. Nevertheless in the SC state we have provided a concrete foundation for the freezing of fluctuating spin correlations by disorder and magnetic field on the same footing; in particular the role of the quasiparticle bound states in the formation of the magnetic order has been highlighted.

The new picture that emerges is complementary to the global competition between SC

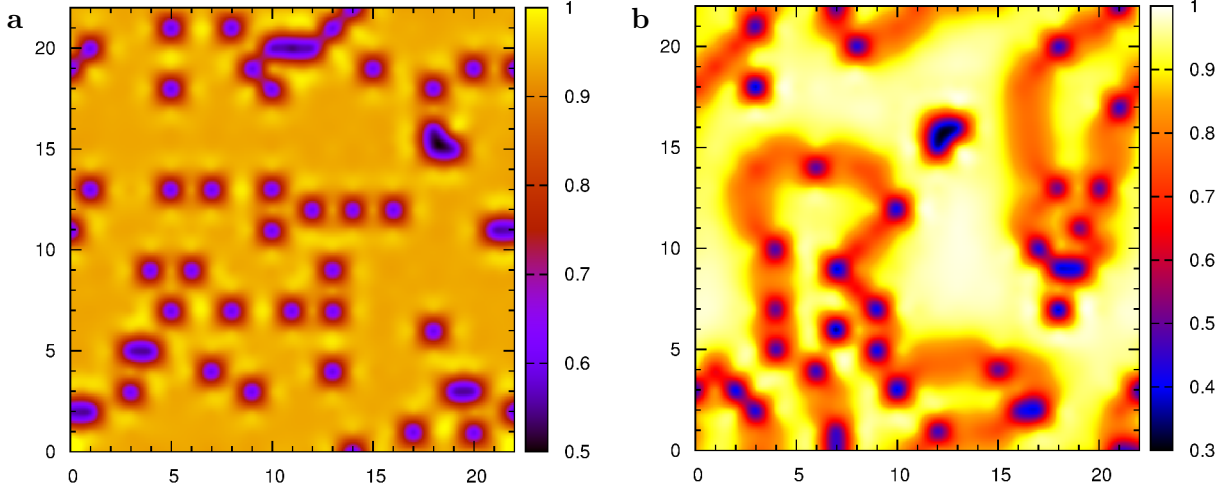


Figure 6: Charge-density profiles. **a.** The same parameter set in zero field as in Fig. 4: $U = 2.9t$, $V_{imp} = 1.3t$, doping $x = 10\% = n^{imp}$, and pairing interaction strength $V_d = 1.34t$. **b.** $U = 4.0t$, $V_{imp} = 1.3t$, doping $x = 15\%$, $n^{imp} = 7.5\%$, and $V_d = 2.0t$. In (a) and (b) the temperature is $T = 0.025t$.

and AF phases in the sense that SC and disorder may significantly enhance SDW order in the underdoped regime. The d -wave pairing of the SC condensate is crucial for this generation of local magnetism, as we have shown. Support for this cooperative effect between SDW and SC comes not only from the onset of the elastic magnetic neutron signal at T_c but also from Zn-substituted optimally doped LSCO. There it is found by μ SR that 2% Zn induces a magnetic signal, but 3% Zn is found to eliminate it, but also destroys superconductivity³¹; within the context of the current theory, this effect is understood not as a consequence of spin dilution³¹, but rather due to the destruction of the SC phase and thereby its ability to generate (or enhance) magnetic order.

Finally we show that a qualitatively different kind of inhomogeneous textures may also be stabilized within the present weak-coupling approach. Figure 6a shows the typical charge-density profile in zero field for a parameter set used above to explore the onset of static AF. As expected, at and near the impurity sites the electron density is reduced, and in these areas the local SDW patches nucleate. With increasing repulsion U and for larger hole densities exceeding the impurity concentration, the inhomogeneous spin and charge patterns change qualitatively, and the impurity-centered patches with reduced electron density evolve into hole-rich filamentary structures (see Fig. 6b). In this still SC state the filaments constitute snake-like paths through an SDW background with an average density of almost one electron

per site. These textures provide a link to the study of disordered (quenched) stripes similar to those discussed recently within various GL models.^{32–34} Therefore, depending upon the correlation strength and the details of the disorder, the magnetic ordering temperature T_g can vary significantly, and the ordering itself can be droplet-like or filamentary-like. This may explain much of the variability of neutron and μSR experiments on different cuprates. Many interesting open questions remain to be addressed in future work, including the possibility of nematic instabilities in the presence of weak symmetry breaking fields and the transfer of spin-fluctuation spectral weight to finite energies in samples where magnetism is not frozen.

APPENDIX A: NUMERICAL METHOD

In order to investigate disorder- and field-induced magnetic order in d -wave superconductors we self-consistently solve the Bogoliubov - de Gennes (BdG) equations on a square lattice for the Hamiltonian

$$\begin{aligned}
H = & - \sum_{ij\sigma} t_{ij} e^{i\varphi_{ij}} c_{i\sigma}^\dagger c_{j\sigma} - \mu \sum_{i\sigma} c_{i\sigma}^\dagger c_{i\sigma} + \sum_{\langle ij \rangle} \left(\Delta_{ij} c_{i\uparrow}^\dagger c_{j\downarrow}^\dagger + h.c. \right) \\
& + \frac{U}{2} \sum_i (\langle n_i \rangle n_i - \langle \sigma_i^z \rangle \sigma_i^z) + \sum_{i\sigma} V_i^{imp} c_{i\sigma}^\dagger c_{i\sigma},
\end{aligned} \tag{A1}$$

where the hopping amplitude between nearest neighbor and next-nearest neighbor sites i and j is described by $t_{ij} = t$ and $t_{ij} = t' = -0.4t$, respectively. An orbital magnetic field is represented by the Peierls phase factor $\varphi_{ij} = (\pi/\Phi_0) \int_{\mathbf{r}_j}^{\mathbf{r}_i} \mathbf{A}(\mathbf{r}) \cdot d\mathbf{r}$, while $\Phi_0 = hc/(2e)$ is the superconducting flux quantum and $\mathbf{A}(\mathbf{r}) = B(0, x)$ is the vector potential of the magnetic field in the Landau gauge. The d -wave pairing potential is defined on two nearest neighbor sites i and j by

$$\Delta_{ij} = -V_d \langle c_{j\downarrow} c_{i\uparrow} \rangle = \Delta_{ji}, \tag{A2}$$

where V_d is the attractive pairing interaction strength, which we set to $V_d = 1.34t$ throughout the paper. We then define a gauge invariant d -wave order parameter on each lattice site i

$$\Delta_i^d = \frac{1}{4} (\Delta_{i,i+\hat{x}}^d + \Delta_{i,i-\hat{x}}^d - \Delta_{i,i+\hat{y}}^d - \Delta_{i,i-\hat{y}}^d), \tag{A3}$$

where $\Delta_{i,j}^d = \Delta_{ij} \exp[-i(\pi/\Phi_0) \int_{\mathbf{r}_j}^{\mathbf{r}_i} \mathbf{A}(\mathbf{r}) \cdot d\mathbf{r}]$. The chemical potential μ is adjusted to fix the average charge density $n = \frac{1}{N} \sum_i \langle n_i \rangle$, while the electron number operator for spin σ at site i

is given by $n_{i\sigma} = c_{i\sigma}^\dagger c_{i\sigma}$, and the local charge-density operator by $n_i = n_{i\uparrow} + n_{i\downarrow}$, respectively. $S_i^z = \frac{1}{2}\sigma_i^z = \frac{1}{2}(n_{i\uparrow} - n_{i\downarrow})$ is the z -component of the spin-operator at site i .

The Bogoliubov transformation

$$c_{i\sigma} = \sum_n \left(u_{in\sigma} \gamma_{n\sigma} + v_{in\sigma}^* \gamma_{n-\sigma}^\dagger \right), \quad (\text{A4})$$

diagonalizes the Hamiltonian in equation (A1), which thereby takes the form

$$H = E_0 + \sum_{n\sigma} E_{n\sigma} \gamma_{n\sigma}^\dagger \gamma_{n\sigma}. \quad (\text{A5})$$

E_0 is the ground-state energy and $\gamma_{n\sigma}^\dagger$ creates an elementary fermionic Bogoliubov quasiparticle excitation with quantum number n , spin σ , and energy $E_{n\sigma} > 0$. Calculation of the commutators of H from equation (A5) with the electron operators $c_{i\sigma}$ leads to a Schrödinger-like set of BdG equations

$$\sum_j \begin{pmatrix} H_{ij}^+ & \Delta_{ij} \\ \Delta_{ij}^* & -H_{ij}^{-*} \end{pmatrix} \begin{pmatrix} u_{jn\uparrow} \\ v_{jn\downarrow} \end{pmatrix} = E_{n\uparrow} \begin{pmatrix} u_{in\uparrow} \\ v_{in\downarrow} \end{pmatrix}, \quad (\text{A6})$$

and

$$\sum_j \begin{pmatrix} H_{ij}^+ & \Delta_{ij} \\ \Delta_{ij}^* & -H_{ij}^{-*} \end{pmatrix} \begin{pmatrix} v_{jn\uparrow}^* \\ u_{jn\downarrow}^* \end{pmatrix} = -E_{n\downarrow} \begin{pmatrix} v_{in\uparrow}^* \\ u_{in\downarrow}^* \end{pmatrix}, \quad (\text{A7})$$

with

$$H_{ij}^\pm = -t_{ij} + \delta_{ij} \left[-\mu + \frac{U}{2} (\langle n_i \rangle \mp \langle \sigma_i^z \rangle) + V_i^{imp} \right]. \quad (\text{A8})$$

As we only search for solutions with positive $E_{n\sigma}$, it is sufficient to solve the following single matrix equation

$$\sum_j \begin{pmatrix} H_{ij}^+ & \Delta_{ij} \\ \Delta_{ij}^* & -H_{ij}^{-*} \end{pmatrix} \begin{pmatrix} u_{jn} \\ v_{jn} \end{pmatrix} = E_n \begin{pmatrix} u_{in} \\ v_{in} \end{pmatrix}, \quad (\text{A9})$$

This is because the solutions for $E_n > 0$ are obviously identical to the solutions for the (positive) eigenvalues $E_{n\uparrow}$ of equation (A6)

$$E_n > 0 : \quad \begin{pmatrix} u_{in\uparrow} \\ v_{in\downarrow} \end{pmatrix} = \begin{pmatrix} u_{in} \\ v_{in} \end{pmatrix} \text{ and } E_{n\uparrow} = E_n > 0, \quad (\text{A10})$$

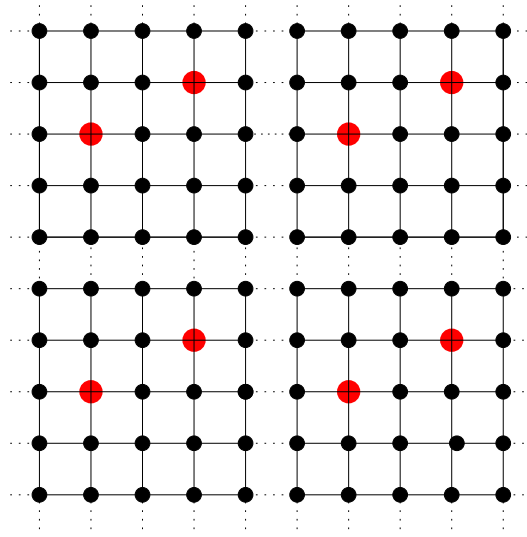


Figure 7: Division of the lattice into identical supercells. Lattice sites belonging to the same supercell are connected via solid lines, while dashed lines link sites of different supercells. Red lattice sites simulate a possibly existing disorder.

while for $E_n < 0$ the following relation holds

$$E_n < 0 : \quad \begin{pmatrix} v_{in\uparrow}^* \\ u_{in\downarrow}^* \end{pmatrix} = \begin{pmatrix} u_{in} \\ v_{in} \end{pmatrix} \text{ and } E_{n\downarrow} = -E_n > 0. \quad (\text{A11})$$

Since the solutions of equations (A6) and (A7) can be mapped on to those of the BdG equation (A9), we diagonalize equation (A9) to obtain the pairing potential Δ_{ij} , the charge density $\langle n_i \rangle$, and the local magnetization $\langle \sigma_i^z \rangle$ self-consistently from

$$\Delta_{ij} = \frac{V_d}{4} \sum_n (u_{in} v_{jn}^* + u_{jn} v_{in}^*) \tanh \left(\frac{E_n}{2k_B T} \right), \quad (\text{A12})$$

$$\langle n_{i\uparrow} \rangle = \sum_n |u_{in}|^2 f(E_n), \quad (\text{A13})$$

$$\langle n_{i\downarrow} \rangle = \sum_n |v_{in}|^2 (1 - f(E_n)), \quad (\text{A14})$$

$$\langle \sigma_i^z \rangle = \langle n_{i\uparrow} \rangle - \langle n_{i\downarrow} \rangle, \quad (\text{A15})$$

where $f(E_n) = (1 + e^{E_n/k_B T})^{-1}$ is the Fermi distribution function and T is the temperature. Sums over n run over positive and negative energies E_n .

To maximize the size of the system for which equation (A9) can be diagonalized numerically, we take advantage of the magnetic translation symmetry of our model Hamiltonian (A1) by dividing the lattice into $M_x \times M_y$ identical supercells each with $N_x \times N_y$ sites (see

Supp. Fig. 7).^{20,35,36} We define the following magnetic translation operator³⁷

$$\mathcal{T}_{\mathbf{R}} = \exp \left(-i \mathbf{R} \cdot \left(\mathbf{k} + \frac{q}{c\hbar} \mathbf{A} \right) \right), \quad (\text{A16})$$

where \mathbf{R} is the translation vector and $\mathcal{T}_{\mathbf{R}}$ translates any lattice vector \mathbf{r} to the position $\mathbf{r} + \mathbf{R}$. Because $[H, \mathcal{T}_{\mathbf{R}}] = 0$, it is possible to block diagonalize the Hamiltonian H in equation (A1) using the eigenstates of $\mathcal{T}_{\mathbf{R}}$. This reduces the eigenvalue problem (A9) of dimension $2M_x N_x \times 2M_y N_y$ to $M_x \times M_y$ eigenvalue equations of dimension $2N_x \times 2N_y$. Applying the magnetic Bloch theorem

$$\begin{pmatrix} u_{n\mathbf{k}}(\mathcal{T}_{\mathbf{R}}\mathbf{r}_i) \\ v_{n\mathbf{k}}(\mathcal{T}_{\mathbf{R}}\mathbf{r}_i) \end{pmatrix} = e^{-i\mathbf{k} \cdot \mathbf{R}} \begin{pmatrix} e^{-i\frac{\pi}{\Phi_0} \mathbf{A}(\mathbf{R}) \cdot \mathbf{r}_i} u_{n\mathbf{k}}(\mathbf{r}_i) \\ e^{i\frac{\pi}{\Phi_0} \mathbf{A}(\mathbf{R}) \cdot \mathbf{r}_i} v_{n\mathbf{k}}(\mathbf{r}_i) \end{pmatrix} \quad (\text{A17})$$

block diagonalizes the BdG equations (A9), where $\mathbf{k} = 2\pi(\frac{n_x}{M_x N_x}, \frac{n_y}{M_y N_y})$, $u_{n\mathbf{k}}(\mathbf{r}_i) = u_{i n\mathbf{k}}$ and $v_{n\mathbf{k}}(\mathbf{r}_i) = v_{i n\mathbf{k}}$. Thus we have to solve the following $2N_x \times 2N_y$ matrix equation for each \mathbf{k} value

$$\sum_j \begin{pmatrix} H_{ij}^+(\mathbf{k}) & \Delta_{ij}(\mathbf{k}) \\ \Delta_{ij}^*(\mathbf{k}) & -H_{ij}^-(\mathbf{k}) \end{pmatrix} \begin{pmatrix} u_{j n\mathbf{k}} \\ v_{j n\mathbf{k}} \end{pmatrix} = E_{n\mathbf{k}} \begin{pmatrix} u_{i n\mathbf{k}} \\ v_{i n\mathbf{k}} \end{pmatrix}, \quad (\text{A18})$$

where

$$\Delta_{ij} = \frac{V_d}{4M_x M_y} \sum_{n\mathbf{k}} (u_{i n\mathbf{k}} v_{j n\mathbf{k}}^* + u_{j n\mathbf{k}} v_{i n\mathbf{k}}^*) \tanh \left(\frac{E_{n\mathbf{k}}}{2k_B T} \right), \quad (\text{A19})$$

$$\langle n_{i\uparrow} \rangle = \frac{1}{M_x M_y} \sum_{n\mathbf{k}} |u_{i n\mathbf{k}}|^2 f(E_{n\mathbf{k}}), \quad (\text{A20})$$

$$\langle n_{i\downarrow} \rangle = \frac{1}{M_x M_y} \sum_{n\mathbf{k}} |v_{i n\mathbf{k}}|^2 (1 - f(E_{n\mathbf{k}})). \quad (\text{A21})$$

H_{ij} and Δ_{ij} are only \mathbf{k} dependent, if i and j belong to different supercells. Then the back-mapping (see Supp. Fig. 8) leads to an additional phase for the u 's and v 's according to (A17), which is assigned to the matrix elements $t_{ij}(\mathbf{k})$ and $\Delta_{ij}(\mathbf{k})$. To make sure that two magnetic translations commute, we have to choose the magnetic field such that its flux through every supercell is a multiple of $2\Phi_0$.^{20,37} Hence $2\Phi_0$ provides a lower boundary for the magnetic flux threading each supercell, which corresponds for a supercell enclosing an area of e.g. $22a \times 22a$ to a magnetic field of about 59 T (we assumed a typical value for the in-plane lattice constant a in the cuprates of about $a = 3.8\text{\AA}$).

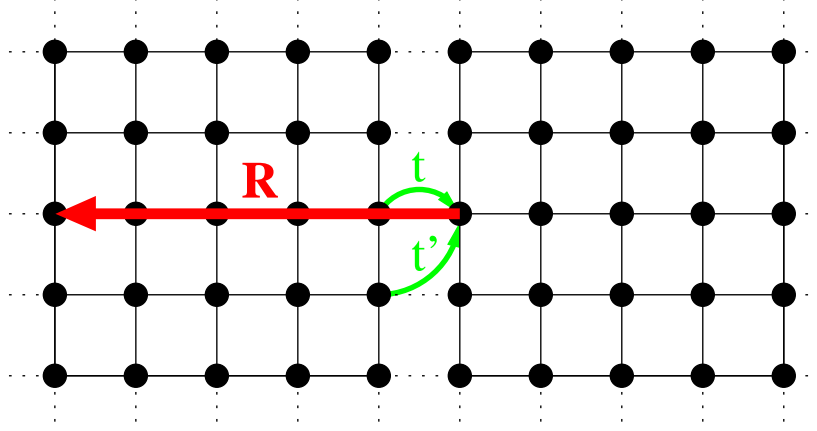


Figure 8: Hopping between supercells. A particle, which hops from the left supercell into the right supercell, is mapped back to the left supercell through the translation vector \mathbf{R} . As a result the wave functions u and v obtain an additional phase given by the magnetic Bloch theorem (A17).

In order to make contact with neutron scattering experiments, we evaluate the magnetic structure factor $S(\mathbf{q})$. In homogeneous systems it is defined as

$$S(\mathbf{q}) = \frac{1}{N} \sum_i \langle \sigma_i^z \sigma_0^z \rangle e^{-i\mathbf{q} \cdot (\mathbf{r}_i - \mathbf{r}_0)}. \quad (\text{A22})$$

We approximate the spin-spin correlation function by the following factorization

$$\langle \sigma_i^z \sigma_0^z \rangle \rightarrow \langle \sigma_i^z \rangle \langle \sigma_0^z \rangle. \quad (\text{A23})$$

Because the system which we are interested in is in general inhomogeneous, we have to sum over all lattice sites. Hence we find the expression

$$|M(\mathbf{q})|^2 = \frac{1}{N^2} \sum_{ij} \langle \sigma_i^z \rangle \langle \sigma_j^z \rangle e^{-i\mathbf{q} \cdot (\mathbf{r}_j - \mathbf{r}_i)}. \quad (\text{A24})$$

This approximation of the magnetic structure factor is identical to the Fourier transform of the magnetization squared.

In Supp. Fig. 9 results for $\langle n_i \rangle$, Δ_i^d , and $\langle \sigma_i^z \rangle$ are shown in zero field (left column) and in finite magnetic field (right column) for a typical impurity configuration. One can identify the location of the impurities by the point-like suppression of the charge density (top row). While the d -wave order parameter is nearly homogeneous in the zero-field case (see Supp. Fig. 9b), one can clearly spot the positions of the two vortices where Δ_i^d is suppressed to zero in Supp. Fig. 9e. In comparison to the zero-field case, a finite orbital magnetic field leads to an additional reduction of the order parameter over the entire lattice.

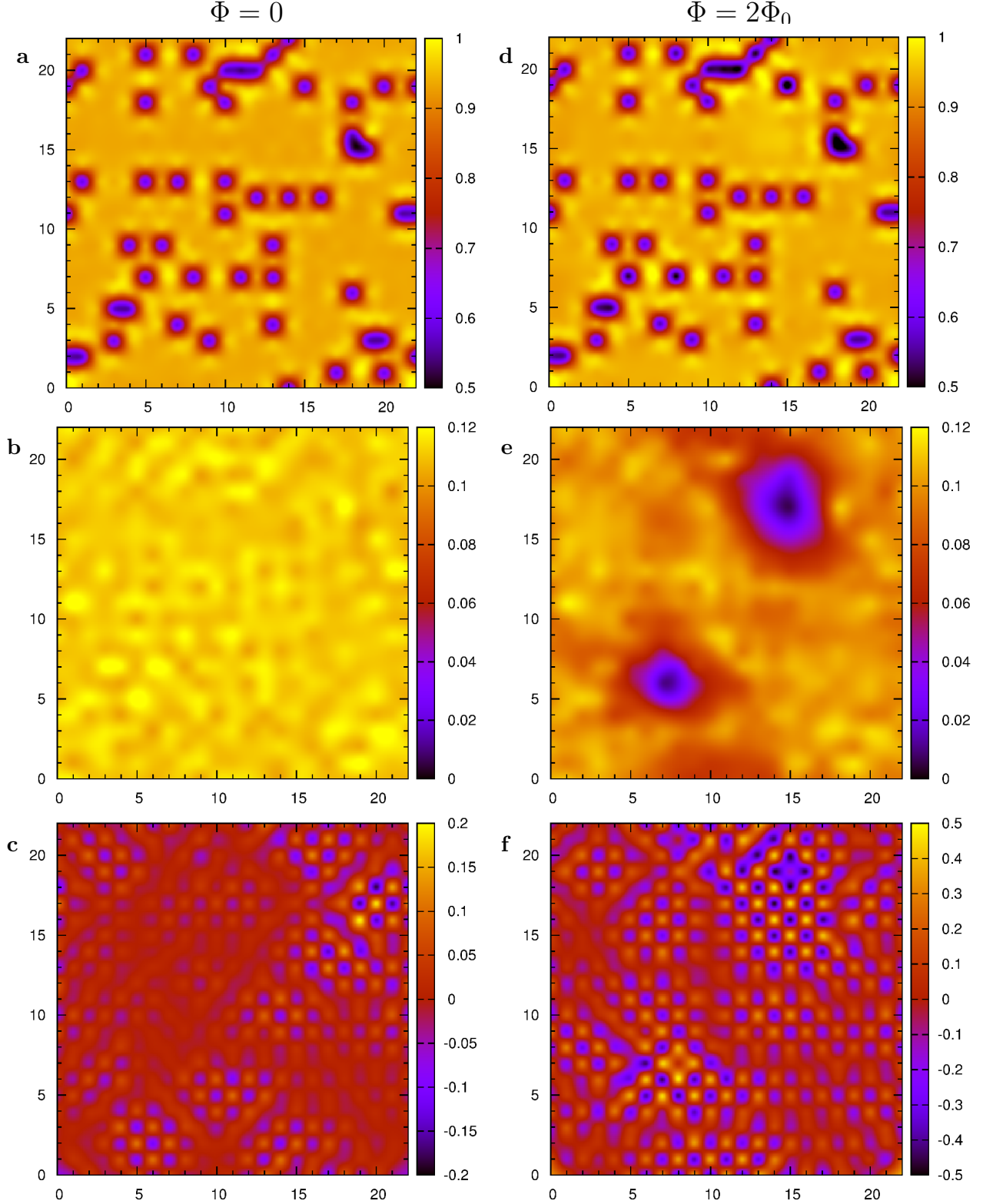


Figure 9: Switching on an orbital magnetic field. **a-c.** Zero-field data. **d-f.** Finite-field data ($\Phi = 2\Phi_0$). **a, d** show the charge density $\langle n_i \rangle$, **b, e** the d -wave order parameter Δ_i^d , and **c, f** the magnetization $\langle \sigma_i^z \rangle$ in real space. The same set of parameters is used here as in the rest of the paper, i.e. $x = 10\% = n_{imp}, U = 2.9t, V_{imp} = 1.3t$. These data were obtained at the lowest temperature $T = 0.025t$ we considered throughout the paper. Note the different scales in **c** and **f**.

Finally, for the parameters used here, the zero field case already contains impurity-induced antiferromagnetic order (see Supp. Fig. **9c**), which is significantly enhanced by switching on a magnetic field. The magnetization peaks near the vortex cores, but due to the fact that strong type-II superconductors are penetrated by the field much beyond the cores, the magnetization is also enhanced in regions far away from the vortices, where the order parameter is nearly homogeneous. The SDW emerges due to the splitting of the Andreev bound state as explained in greater detail in the main body of the paper.

References

- 1 Sachdev, S. Colloquium: Order and quantum phase transitions in the cuprate superconductors, *Rev. Mod. Phys.* **75**, 913 (2003).
- 2 Lake, B. *et al.* Antiferromagnetic order induced by an applied magnetic field in a high-temperature superconductor. *Nature* **415**, 299 (2002).
- 3 Haug, D. *et al.* Magnetic-field-enhanced incommensurate magnetic order in the underdoped high-temperature superconductor $\text{YBa}_2\text{Cu}_3\text{O}_{6.45}$. *Phys. Rev. Lett.* **103**, 017001 (2009).
- 4 Chang, J. *et al.* Tuning competing orders in $\text{La}_{2-x}\text{Sr}_x\text{CuO}_4$ cuprate superconductors by the application of an external magnetic field. *Phys. Rev. B* **78**, 104525 (2008).
- 5 Khaykovich, B. *et al.* Enhancement of long-range magnetic order by magnetic field in superconducting $\text{La}_2\text{CuO}_{4+y}$. *Phys. Rev. B* **66**, 014528 (2002).
- 6 Khaykovich, B. *et al.* Field-induced transition between magnetically disordered and ordered phases in underdoped $\text{La}_{2-x}\text{Sr}_x\text{CuO}_4$. *Phys. Rev. B* **71**, 220508 (2005).
- 7 Hoffman, J. E. *et al.* A four unit cell periodic pattern of quasi-particle states surrounding vortex cores in $\text{Bi}_2\text{Sr}_2\text{CaCu}_2\text{O}_{8+\delta}$. *Science* **295**, 466 (2002).
- 8 Panagopoulos, C. *et al.* Evidence for a generic quantum transition in high- T_c cuprates. *Phys. Rev. B* **66**, 064501 (2002).
- 9 Niedermayer, Ch. *et al.* Common phase diagram for antiferromagnetism in $\text{La}_{2-x}\text{Sr}_x\text{CuO}_4$ and $\text{Y}_{1-x}\text{Ca}_x\text{Ba}_2\text{Cu}_3\text{O}_6$ as seen by muon spin rotation. *Phys. Rev. Lett.* **80**, 3843 (1998).
- 10 Kivelson, S. A. *et al.* How to detect fluctuating stripes in the high-temperature superconductors. *Rev. Mod. Phys.* **75**, 1201 (2003).

- 11 Andersen, B. M., Hirschfeld, P. J., Kampf, A. P. & Schmid, M. Disorder-induced static anti-ferromagnetism in cuprate superconductors. *Phys. Rev. Lett.* **99**, 147002 (2007).
- 12 Harter, J. W. *et al.* Antiferromagnetic correlations and impurity broadening of NMR linewidths in cuprate superconductors. *Phys. Rev. B* **75**, 054520 (2007).
- 13 Tsuchiura, H., Tanaka, Y., Ogata, M. & Kashiwaya, S. Local magnetic moments around a nonmagnetic impurity in the two-dimensional t-J model. *Phys. Rev. B* **64**, 140501 (2000).
- 14 Wang, Z. & Lee, P. A. Local moment formation in the superconducting state of a doped Mott insulator. *Phys. Rev. Lett.* **89**, 217002 (2002).
- 15 Alloul, H., Bobroff, J., Gabay, M. & Hirschfeld, P. J. Defects in correlated metals and superconductors. *Rev. Mod. Phys.* **81**, 45 (2009).
- 16 Kimura, H., Kofu, M., Matsumoto, M. Y. & Hirota, K. Novel in-gap spin state in Zn-doped $\text{La}_{1.85}\text{Sr}_{0.15}\text{CuO}_4$. *Phys. Rev. Lett.* **91**, 067002 (2003).
- 17 Demler, E., Sachdev, S. & Zhang, Y. Spin-ordering quantum transition of superconductors in a magnetic field. *Phys. Rev. Lett.* **87**, 067202 (2001).
- 18 Wang, Y. & MacDonald, A. H. Mixed-state quasiparticle spectrum for d-wave superconductors. *Phys. Rev. B* **52**, R3876 (1995).
- 19 Andersen, B. M., Bruus, H., & Hedegård, P. SO(5) Theory of Insulating Vortex Cores in High T_c Materials. *Phys. Rev. B* **61**, 6298 (2000).
- 20 Zhu, J.-X. & Ting, C. S. Quasiparticle states at a d-wave vortex core in high- T_c superconductors: induction of local spin density wave order. *Phys. Rev. Lett.* **87**, 147002 (2001).
- 21 Chen, Y. & Ting, C. S. Magnetic-field-induced spin-density wave in high-temperature superconductors. *Phys. Rev. B* **65**, 180513 (2002).
- 22 Zhu, J.-X., Martin, I. & Bishop, A. R. Spin and charge order around vortices and impurities in high- T_c superconductors. *Phys. Rev. Lett.* **89**, 067003 (2002).
- 23 Maggio-Aprile, I. *et al.* Direct vortex lattice imaging and tunneling spectroscopy of flux lines on $\text{YBa}_2\text{Cu}_3\text{O}_{7-\delta}$. *Phys. Rev. Lett.* **75**, 2754 (1995).
- 24 Pan, S. H. *et al.* STM studies of the electronic structure of vortex cores in $\text{Bi}_2\text{Sr}_2\text{CaCu}_2\text{O}_{8+\delta}$. *Phys. Rev. Lett.* **85**, 1536 (2000).
- 25 Pan, S. H. *et al.* Imaging the effects of individual zinc impurity atoms on superconductivity in $\text{Bi}_2\text{Sr}_2\text{CaCu}_2\text{O}_{8+\delta}$. *Nature* **403**, 746 (2000).
- 26 Doiron-Leyraud, N. *et al.* Quantum oscillations and the Fermi surface in an underdoped high- T_c

- superconductor. *Nature* **447**, 565 (2007).
- 27 LeBoeuf, D. *et al.* Electron pockets in the Fermi surface of hole-doped high- T_c superconductors. *Nature* **450**, 533 (2007).
 - 28 Damascelli, A., Hussain, Z. & Shen, Z. X. Angle-resolved photoemission studies of the cuprate superconductors. *Rev. Mod. Phys.* **75**, 473 (2003).
 - 29 Shender, E. F. & Kivelson, S. A. Dilution-induced order in quasi-one-dimensional quantum antiferromagnets. *Phys. Rev. Lett.* **66**, 2384 (1991).
 - 30 For a review, see J. M. Tranquada, in *Handbook of High-Temperature Superconductivity Theory and Experiment*, edited by J. R. Schrieffer (Springer, New York, 2007).
 - 31 Watanabe, I. *et al.* Muon-spin-relaxation study of the effect of nonmagnetic impurities on the Cu-spin fluctuations in $\text{La}_{2-x}\text{Sr}_x\text{Cu}_{1-y}\text{Zn}_y\text{O}_4$ around $x = 0.115$. *Phys. Rev. B* **65**, 180516(R) (2002).
 - 32 Robertson, J. A. *et al.* Distinguishing patterns of charge order: Stripes or checkerboards. *Phys. Rev. B* **74**, 134507 (2006).
 - 33 Del Maestro, A., Rosenow, B. & Sachdev, S. From stripe to checkerboard ordering of charge-density waves on the square lattice in the presence of quenched disorder. *Phys. Rev. B* **74**, 024520 (2006).
 - 34 Vojta, M., Lattice symmetry breaking in cuprate superconductors: stripes, nematics, and superconductivity. *Adv. Phys.* **58**, 699 (2009).
 - 35 Ghosal, A., Kallin, C. & Berlinsky, A. J. Competition of superconductivity and antiferromagnetism in a d -wave vortex lattice. *Phys. Rev. B* **66**, 214502 (2002).
 - 36 Atkinson, W. A. & Sonier, J. E. Role of CuO chains in vortex core structure in $\text{YBa}_2\text{Cu}_3\text{O}_{7-\delta}$. *Phys. Rev. B* **77**, 024514 (2008)
 - 37 Brown, E. Bloch electrons in a uniform magnetic field. *Phys. Rev.* **133**, A1038 (1964).

Acknowledgements

This work was supported by the DFG through SFB 484 (M.S. and A.P.K.), by The Danish Council for Independent Research | Natural Sciences (B.M.A.), and by the DOE under grant DE-FG02-05ER46236 (P.J.H.).